

See discussions, stats, and author profiles for this publication at: <https://www.researchgate.net/publication/261880677>

Metal–Organic Frameworks with Mechanically Interlocked Pillars: Controlling Ring Dynamics in the Solid–State via a Reversible Phase Change

ARTICLE in JOURNAL OF THE AMERICAN CHEMICAL SOCIETY · APRIL 2014

Impact Factor: 12.11 · DOI: 10.1021/ja502238a · Source: PubMed

CITATIONS

21

READS

37

5 AUTHORS, INCLUDING:



Kelong Zhu

University of Windsor

32 PUBLICATIONS 904 CITATIONS

[SEE PROFILE](#)



Vedran Nicholas Vukotic

PROTO Manufacturing

24 PUBLICATIONS 441 CITATIONS

[SEE PROFILE](#)



Robert Schurko

University of Windsor

108 PUBLICATIONS 2,014 CITATIONS

[SEE PROFILE](#)



Stephen Joseph Loeb

University of Windsor

162 PUBLICATIONS 4,319 CITATIONS

[SEE PROFILE](#)

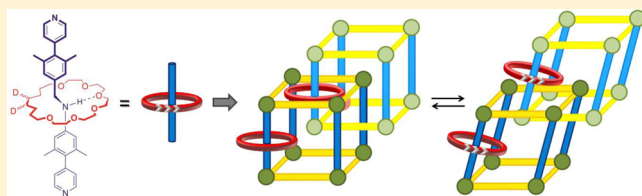
Metal–Organic Frameworks with Mechanically Interlocked Pillars: Controlling Ring Dynamics in the Solid-State via a Reversible Phase Change

Kelong Zhu, V. Nicholas Vukotic, Christopher A. O’Keefe, Robert W. Schurko,* and Stephen J. Loeb*

Department of Chemistry and Biochemistry, University of Windsor, Windsor, Ontario Canada, N9B 3P4

Supporting Information

ABSTRACT: Metal–organic framework (MOF) materials have been prepared that contain a mechanically interlocked molecule (MIM) as the pillaring strut between two periodic Zn-carboxylate layers. The MIM linker is a [2]rotaxane with a [24]crown-6 (24C6) macrocycle and an aniline-based axle with terminal pyridine donor groups. The single-crystal X-ray structures of MOFs UWDM-2 (1,4-diazophenyl-dicarboxylate) and UWDM-3 (1,4-biphenyl-dicarboxylate) show that both frameworks are large enough to contain the free volume required for rotation of the interlocked 24C6 macrocycle, but the frameworks are interpenetrated (UWDM-2, three-fold, and UWDM-3, two-fold). In particular, for UWDM-3 the 24C6 rings of the pillaring MIM are positioned directly inside the square openings of neighboring zinc dicarboxylate layers. Variable-temperature (VT) ^2H SSNMR demonstrated that the 24C6 macrocycles in UWDM-2 and UWDM-3 can only undergo restricted motions related to ring flexibility or partial rotation but are incapable of undergoing free rotation. VT-powder X-ray diffraction studies showed that upon activation of UWDM-3, by removing solvent, a phase change occurs. The new β -phase of UWDM-3 retained crystallinity, and ^2H SSNMR demonstrated that the 24C6 macrocyclic ring of the pillared MIM strut is now free enough to undergo full rotation. Most importantly, the phase change is reversible; the β version of the MOF can be reverted to the original α state by resolvation, thus demonstrating, for the first time, that the dynamics of a MIM inside a solid material can be controlled by a reversible phase change.



1. INTRODUCTION

Molecular switches based on mechanically interlocked molecules (MIMs) function well in controlled solution environments,¹ but in this medium their motion is incoherent, and the molecules widely dispersed. In an effort to achieve a higher level of molecular organization and create functional materials employing interlocked components, it has been suggested that MIMs could be organized inside the pores of metal–organic framework (MOF) materials.² To this end, we recently reported a prototype MOF, UWDM-1, which contains a large and flexible [24]crown-6 (24C6) macrocycle interlocked onto a rigid aromatic framework and demonstrated that upon activation of the material, free volume is created inside the pores of the material, and thermally driven rotation of the macrocycle can be observed directly by ^2H SSNMR.³ We believe the next steps in this chemistry are to learn how the internal structure of the MOF affects the motion exhibited by the interlocked macrocycle, and more importantly, how to achieve control over the motion.

Herein, we report a new type of MIM-pillared MOF and show how changing the internal structure of the MOF can affect the type of motion (e.g., conformational flexing, partial rotation, or full rotation) exhibited by the macrocycle. Most importantly, we demonstrate for the first time that these large amplitude dynamics associated with a MIM linker can be

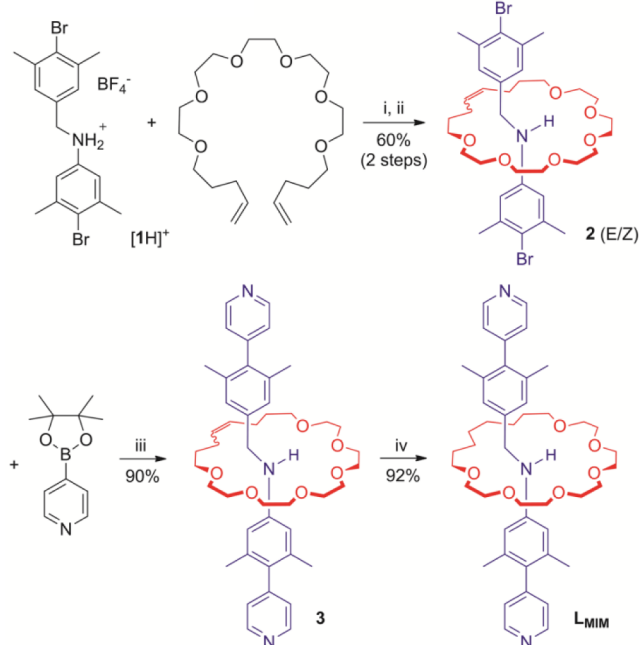
controlled by an external perturbation; in this case via a reversible phase change of the material.

2. RESULTS AND DISCUSSION

MIM Pillaring Ligand. Scheme 1 outlines the synthesis of the pillaring ligand L_{MIM} used in the construction of these hybrid linker MOFs. Ring closing metathesis⁴ was used to create a 24-membered macrocycle around an anilinium-based axle with 4-bromo substituted xylene groups as the stoppers. A standard Suzuki coupling protocol was then used to replace the bromine atoms with 4-pyridyl groups in good yield. Finally, the double bond of the macrocycle (E and Z isomers) could be hydrogenated (or deuterated) employing H_2 (D_2) gas and Pd/C. The structure of the neutral L_{MIM} was determined by single-crystal X-ray diffraction (XRD) and is shown in Figure 1. The length of this new bipyridine ligand is 17.3 Å (N···N), while the diameter around the central macrocycle is ca. 11.2 Å. A single NH hydrogen-bond (N···O 3.44 Å; NH···O, 160°) is the major noncovalent interaction remaining after removal of the templating anilinium charge. The four methyl groups prevent unthreading of the 24-membered ring, thus ensuring the

Received: March 4, 2014

Scheme 1. Synthesis of a MIM Ligand (L_{MIM}) Designed for Pillaring inside a MOF^a



^a(i) Grubbs' first-generation catalyst, CH_3NO_2/CH_2Cl_2 (1:9), 48 h, reflux; (ii) NEt_3/CH_3OH ; (iii) catalytic $Pd(PPh_3)_4$, DMF/toluene, 12 h, 110 °C; and (iv) 10% Pd/C , H_2 (or D_2), CH_3OH , 3 h, RT.

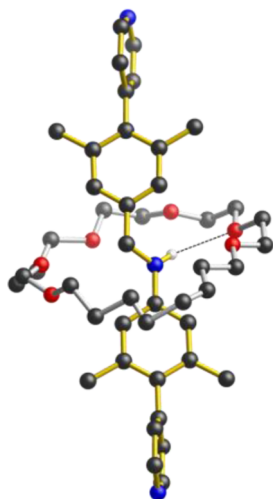


Figure 1. A ball-and-stick representation of the single-crystal X-ray structure of the bipyridine, pillaring ligand L_{MIM} showing a single $NH \cdots O$ interaction between the axle and wheel components. Color key: red = oxygen, blue = nitrogen, black = carbon; gold bonds = axle; silver bonds = wheel.

[2]rotaxane remains a permanently interlocked entity throughout synthesis and postsynthetic modification of the MOF.

MOF Materials. It has been well established by Kim,⁵ Hupp,⁶ and others⁷ that linear bipyridine ligands can be used as pillaring struts between two-periodic layers of zinc carboxylate paddlewheel structures to form robust MOFs. In fact, varying the complexity of this pillaring ligand has been a popular strategy for the incorporation of functional groups into MOFs.⁸ Following the same solvo-thermal protocols, ligand L_{MIM} was combined with $Zn(NO_3)_2 \cdot (H_2O)_x$ and 2 equiv of a dicarboxylic

acid. Of the three acid linkers utilized, 4,4'-azodiphenyl-dicarboxylic acid (ADC), 2,6-naphthyl-dicarboxylic acid (NDC), and 4,4'-biphenyldicarboxylic acid (BPDC), good yields of a MOF were obtained only with the longer acids ADC and BPDC. It was rationalized that since the shorter NDC linker would produce a $Zn \cdots Zn$ distance of only 13.0 Å in the two-periodic layer there would be steric interactions between macrocycles of adjacent L_{MIM} pillars, and this ultimately prevented formation of the target pillared MOF. On the other hand, analogous spacings of 15.2 and 17.0 Å for BPDC and ADC, respectively, were large enough to accommodate side-by-side alignment of [2]rotaxane pillars; thus, formation of a pillared MOF material was successful as designed.

The two MOFs with bridging dicarboxylate linkers ADC and BPDC were designated UWDM-2 and UWDM-3 (UWDM = University of Windsor Dynamic Material), respectively, and isolated as homogeneous materials in good yield with formulas $[Zn_2(BPDC)_2(L_{MIM})](DMF)_2$ and $[Zn_2(ADC)_2(L_{MIM})](DMF)_13$ (see SI for details). Both were analyzed by single-crystal X-ray analysis, and the structures of the basic frameworks are shown in Figure 2.

As designed, the framework structures of UWDM-2 and UWDM-3 consist of two-periodic grids constructed from $Zn(II)$ paddlewheels and carboxylate ligands with the bipyridine ligand L_{MIM} pillaring the layers. Although the structures appear to contain large openings sufficient for potentially unimpeded motion of the interlocked macrocycles as desired, both of these structures are interpenetrated; UWDM-2 is three-fold interpenetrated, while UWDM-3 is two-fold interpenetrated.

Drawings depicting the interpenetration of the lattices for UWDM-2 and UWDM-3 are in Figure 3. For UWDM-2, the 24C6 ring is positioned to one corner and slightly above the square grid defined by the Zn -carboxylate grid. For UWDM-3, two-fold interpretation actually places the macrocyclic 24C6 ring directly inside the Zn -carboxylate square framework—akin to a “round peg in a square hole”. It is quite clear from examination of these solid-state structures that in both cases the 24C6 macrocycles are tightly packed on account of being positioned close to the square grid framework and the lack of any large internal voids due to interpenetrations.

Unit cells for UWDM-2 and UWDM-3 were calculated (PLATON)⁹ to contain void spaces of 17 and 50% occupied by 8 and 104 molecules of DMF, respectively. Thermal gravimetric analysis showed gradual weight loss attributable to DMF removal and eventual decomposition of the MOF frameworks at 370 and 250 °C, respectively (see SI for details).

The stability of UWDM-2 was verified by powder X-ray diffraction (PXRD) which showed very little variation when the material was dried under vacuum (Figure 4). Interestingly, however, VT-PXRD for UWDM-3 demonstrated that this material (α -UWDM-3) goes through a gradual phase change over the temperature range of 100–125 °C (Figure 5), resulting in a second, stable crystalline phase (β -UWDM-3).

The new β -UWDM-3 phase can be attributed to desolvation and tilting of the pillaring strut which brings the carboxylate layers closer together and reduces the volume accessible for solvent molecules. This type of deformation is a known structural feature for a number of similar pillared/layered MOFs.¹⁰ Unfortunately, attempts to index this new phase (DICVOL, DASH)¹¹ and unambiguously determine cell parameters for β -UWDM-3 were not successful due to the broadness of the PXRD patterns. This α to β phase change can

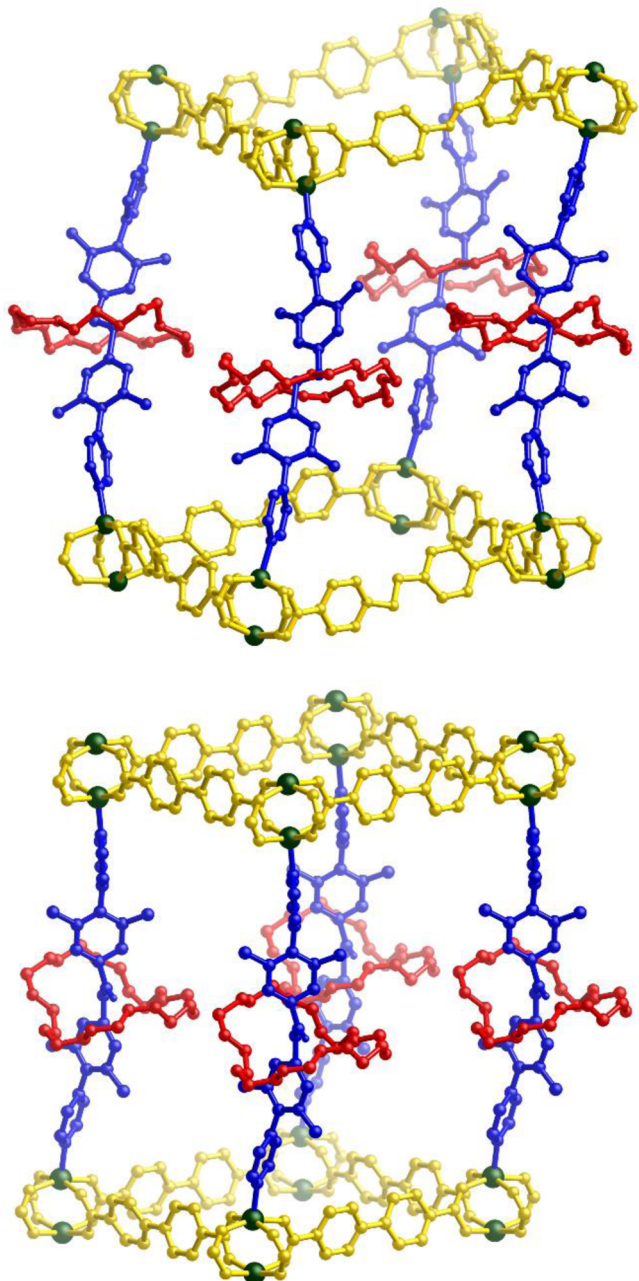


Figure 2. Ball-and-stick representations of the single-crystal X-ray structures of UWDM-2 (top) containing ADC linkers and UWDM-3 (bottom) containing BPDC linkers, showing a portion of one of the interpenetrated lattice frameworks. Color key: blue = aniline axle, red = 24C6 wheel, yellow = carboxylate linkers, green = zinc atoms.

also be initiated by solvent exchange with CH_2Cl_2 and gentle drying of the sample. Most importantly, the phase change can be reversed by re-exposure of the desolvated sample to DMF as shown in Figure 5.

Dynamics in the Solid State. In order to characterize the mobility of the macrocyclic 24C6 rings inside these MOFs, UWDM-2 and UWDM-3 were prepared containing deuterium labels via the addition of D_2 to the double bond created by RCM and the resulting materials probed by ^2H SSNMR. ^{12}C ^2H SSNMR powder patterns are extremely sensitive to molecular-level dynamical motions and act as exquisite probes of changes in the types of motions and their rates that arise from variation

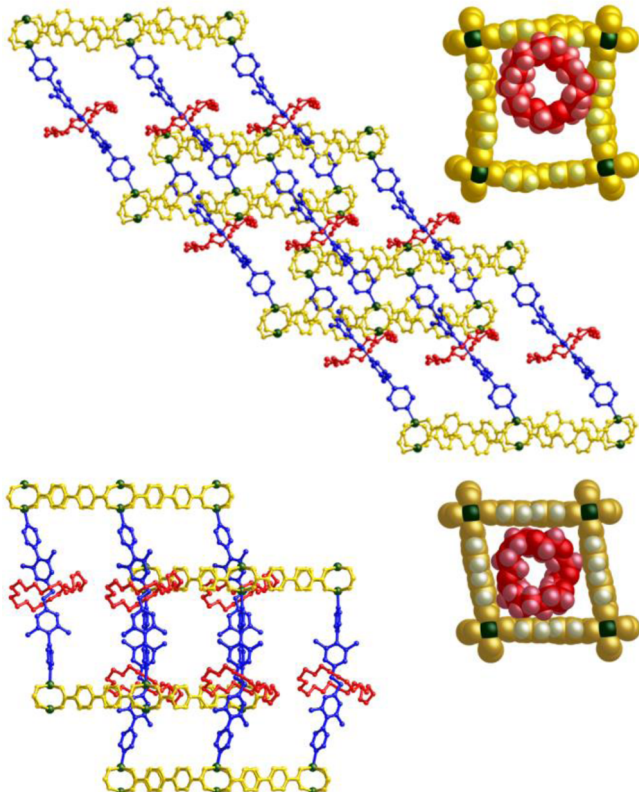


Figure 3. Ball-and-stick representations of the single-crystal X-ray structures of UWDM-2 (top) and UWDM-3 (bottom) showing the interpenetrated lattice frameworks (UWDM-2 is three-fold interpenetrated, and UWDM-3 is two-fold interpenetrated). Space filling models show the position of the macrocycle relative to the square framework grid. Color key: blue = aniline axle, red = 24C6 wheel, yellow = carboxylate linkers, green = zinc atoms.

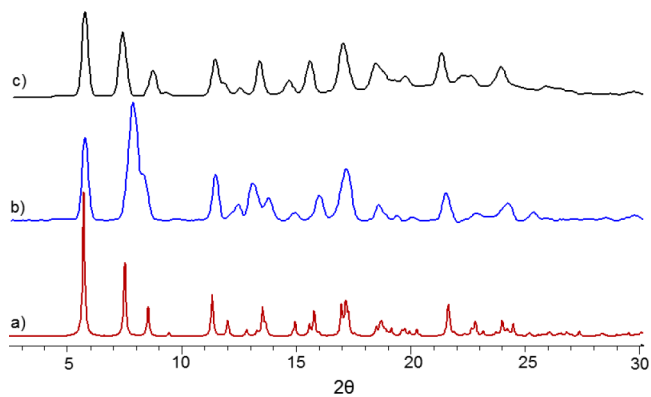


Figure 4. PXRD patterns for UWDM-2: (a) simulated from single-crystal XRD data; (b) as-synthesized material; and (c) exchanged with CH_2Cl_2 and dried in vacuum at RT for 6 h.

in temperature. Three motional regimes are defined on the basis of the typical range of magnitudes of the ^2H quadrupolar coupling constant for terminal C–D bonds (i.e., 100–180 kHz): the slow motion limit (SML), where rates are $<10^3$ Hz; the intermediate motion regime (IMR), where rates are between 10^4 and 10^7 Hz; and the fast motion limit (FML), where rates are $>10^7$ Hz. Motions in the SML and FML can effectively be modeled as time averages of the three principal components of the ^2H electric field gradient (EFG) tensor, whereas motions in the IMR require modeling with an

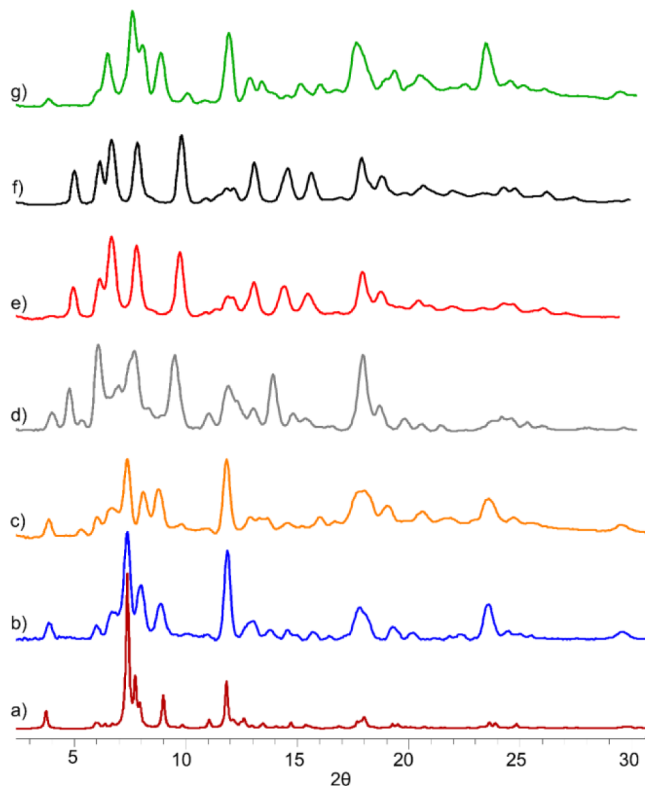


Figure 5. PXRD patterns for UWDM-3 at various temperatures: (a) simulated from single-crystal XRD data; as-synthesized material at (b) 25, (c) 50, (d) 100, and (e) 125 °C; (f) after exchange of solvent from DMF to CH_2Cl_2 and then drying under vacuum at room temperature, (g) sample (f) at 25 °C after soaking in DMF for 12 h.

exchange matrix and generally result in powder patterns of increasing complexity that vary with both changes in temperature and echo spacing. Details of the simulations including tables of relevant rates can be found in the SI.

For UWDM-2, which utilizes the longest ADC linker, three-fold interpenetration occurs which severely restricts the possible motion of the **24C6** macrocycle. Indeed, any large amplitude ring flexing would likely result in significant, unfavorable interactions between the rings. The static spectrum acquired at 171 K was simulated as a single site using quadrupolar parameters that are typical for (i.e., $C_Q = 165$ kHz and $\eta_Q = 0.0$) this type of C–D alkyl linkage. At this temperature, motion of the crown ethers is too slow to affect the ^2H powder patterns, i.e., the slow motion limit. Increasing the temperature to ca. 255 K caused variations in the powder pattern shapes which indicate that motions were occurring at a rate of $\sim 10\text{--}100$ kHz, well within the IMR. The spectra were simulated using a two-site jump of the CD_2 group with an angle of 72° (Figure 6b) combined with a partial rotation motion, which is rotation of the macrocycle through 225° in 45° steps, such that there is a single hydrogen-bonding contact between the pillar and macrocycle (Figure 6c). This motion is described as a partial rotation, since the macrocycle is not free to make a complete rotation about the pillar. The sites are connected such that successive jumps can occur in either direction, but only to adjacent oxygen atoms on the ring and not through the alkyl portion of the macrocycle. The rate of the two-site jump motion is lower than that of the partial ring rotation, as the conformational changes induced in the ring from the latter result in steric interactions between rings. The patterns narrow

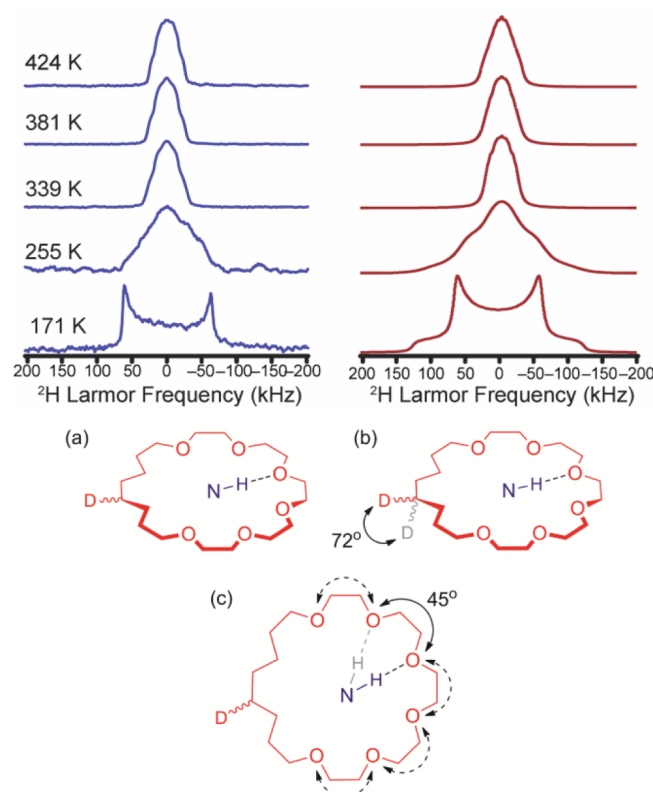


Figure 6. Experimental (left) and simulated (right) ^2H SSNMR powder patterns as a function of temperature for UWDM-2. Illustrations (below) of the motions of the **24C6** macrocyclic ring relative to the framework axle: (a) the SML where no motion is occurring on the NMR time scale, (b) the FML for jumps between two sites 72° apart, and (c) partial rotation of the ring over 225° in 45° steps.

considerably, but at the high-temperature limit (424 K) begin to broaden again. Ratcliffe et al. observed a similar phenomenon for solid complexes of [18]crown-6.¹³ That this hindered motion (i.e., two-site jumps and partial rotation motion) does not occur at rates in the FML is consistent with the constrained nature of the ring in this system.

Although the single-crystal X-ray structure of α -UWDM-3 showed that this framework is only two-fold interpenetrated, the **24C6** ring is confined within a square of the zinc-carboxylate grid. It was therefore postulated that interactions between the ring and the framework would also hinder the motion of the ring in this material. The experimental and simulated VT ^2H SSNMR spectra for α -UWDM-3 are shown in Figure 7. The low-temperature spectrum collected at 234 K was simulated with a single set of quadrupolar parameters (*vide supra*). This SML spectrum was obtained at a higher temperature than that previously observed for UWDM-1, suggesting that the motions of the **24C6** ring in α -UWDM-3 are indeed hindered by comparison.

Increasing the temperature to 247 K produced a distinct spectrum that could be simulated as a two-site jump of the CD_2 groups between sites separated by an angle of 75° (Figure 7b). At 255 K, the width of the spectrum is less than half that of the low-temperature spectrum, indicating that the lone two-site jump model can no longer be used. Collecting spectra at this temperature with different pulse spacings also produced notable changes in the powder pattern; thus, it can be concluded that

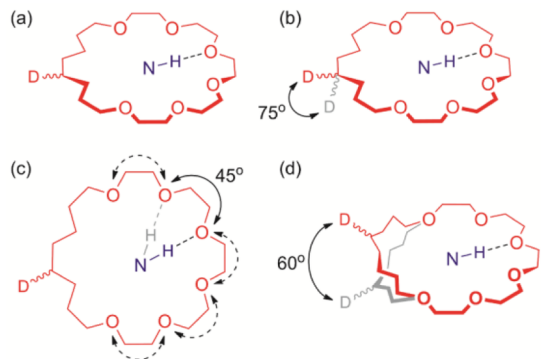
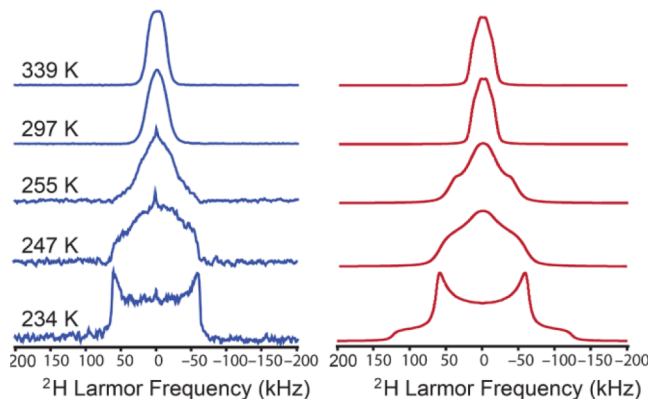


Figure 7. Experimental (left) and simulated (right) ^2H SSNMR powder patterns as a function of temperature for α -UWDM-3. Illustrations (below) of the motions of the 24C6 macrocyclic ring relative to the framework axle: (a) the SML where no motion is occurring on the NMR time scale; (b) the FML for jumps between two sites 75° apart; (c) partial rotation of the ring over 225° in 45° steps; and (d) large amplitude jumps of the alkyl portion of the ring through 60° between positions above and below the square of the framework.

the rates of the new motions are within the IMR. The spectrum was simulated by considering the two-site jump of the CD₂ groups and the onset of partial rotation, as described above for UWDM-2.

Further increasing the temperature produced significantly narrower patterns that could not be accounted for with only a combination of two-site jumps and partial ring rotation. The ^2H NMR spectra acquired at 318 and 339 K were simulated by including a third mode of motion: large amplitude jumps of the deuterons through an angle of 60° about an axis in the plane of the ring (Figure 7d). This motion was attributed to the flexible alkyl portion of the ring moving 60° between positions above and below the constraining square of the Zn-carboxylate layer without significantly altering the length of the NH···O hydrogen bonds, in order to minimize short-range interactions between the macrocyclic ring and the surrounding framework.

For β -UWDM-3, it is postulated that the macrocycle no longer sits within the square of the Zn-carboxylate framework and that the 24C6 ring is more mobile in this less constrained environment. This notion is supported by the VT ^2H SSNMR spectra which are strikingly similar to those previously observed for UWDM-1 (see SI for a detailed comparison). The static spectrum at 183 K was simulated as a single site, and increasing the temperature to 208 K resulted in no significant change in the powder pattern (Figure 8a). The spectrum acquired at 234 K indicates the onset of motion, and the spectrum at 255 K was

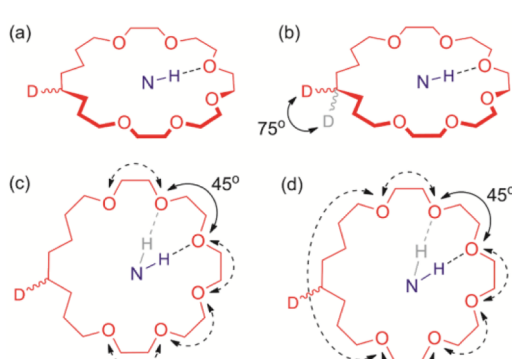
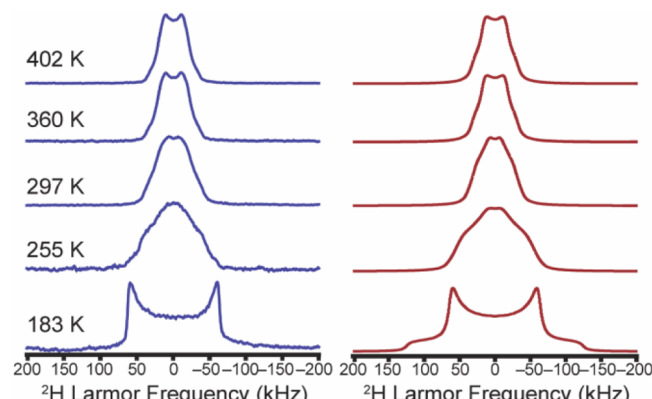


Figure 8. Experimental (left) and simulated (right) ^2H SSNMR powder patterns as a function of temperature for β -UWDM-3. Illustrations (below) of the motions of the 24C6 macrocyclic ring relative to the framework axle: (a) the SML where no motion is occurring on the NMR time scale; (b) the FML for jumps between two sites 75° apart; (c) partial rotation of the ring over 225° in 45° steps; and (d) partial rotation of the ring over 225° in 45° steps combined with jumps over the alkyl portion of the ring resulting in full rotation.

simulated using the familiar two-site jump of the CD₂ groups through an angle of 75° (Figure 8b). Increasing the temperature further induces the onset of partial rotation motion through 225° in 45° increments (Figure 8c), in addition to the aforementioned two-site jump motion. The spectrum at 318 K was simulated with rates in the FML for this combined motion. The temperature at which this mode of motion occurs is similar to that of UWDM-1 (324 K), again validating the congruous motions in these two systems.

The spectra acquired at higher temperatures could not be simulated using the combined two-site jump and partial rotation model, nor could they be simulated with free rotation of the crown ether ring about an axis of $C_n \geq 3$ symmetry. The simulation of the high temperature spectra was achieved by considering a combination of motions best described as full rotation (i.e., an intermediate case between partial rotation and free rotation) combined with the two-site jump. Specifically, eight sites separated by 45° rotations were used: six corresponding to the hydrogen-bonding oxygen atom positions and two corresponding to the alkyl portion of the ring (Figure 8d). A rate matrix was constructed (see SI) where jumps between the oxygen atom positions are occurring at rates in the FML (i.e., $>10^7$ Hz) and jumps through the alkyl positions occur at a significantly slower rate in the IMR (i.e., 50–1000 kHz). The spectra acquired at 381 and 402 K were simulated

using this model, and excellent agreement with the experimental data was obtained.

3. CONCLUSIONS

It has been demonstrated that the dynamic motion of a macrocyclic wheel inside a MOF can be controlled by a reversible phase change in the framework of the material; this concept is illustrated in Figure 9. It is not surprising that the

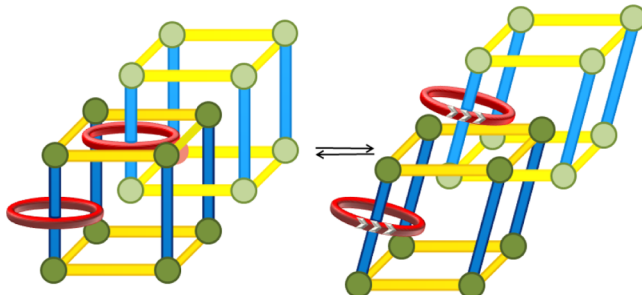


Figure 9. Schematic illustrating the conversion between the as-synthesized α -form (left) and desolvated β -form (right) of UWDM-3 which is accompanied by release of the macrocyclic wheel into a free volume space within the MOF allowing for the full range of dynamic motions as observed by ^2H SSNMR. Color key: blue = axle, red = wheel, yellow = carboxylate linkers, green = zinc atoms.

extent to which the large macrocyclic **24C6** ring can undergo motion is severely restricted when the ring is positioned inside the square opening of the MOF framework as is shown in Figure 3 for the X-ray structures of UWDM-2 and α -UWDM-3. However, when α -UWDM-3 is converted to β -UWDM-3, the change in layer spacing frees the crown ether from being trapped inside the square grid of the framework and allows for thermally driven full rotation of the macrocycle similar to previously reported for UWDM-1.

This new MIM ligand design combined with the successful preparation of robust, pillared MOFs, and the characterization of the internal motion of the interlocked rings in the solid state is a significant step toward the ultimate goals of organizing sophisticated molecular switches and machines inside crystalline solid-state materials and controlling their function therein.

■ ASSOCIATED CONTENT

Supporting Information

Experimental details describing the synthesis and characterization of all new compounds including solution NMR assignments, full characterization details for all new materials, and the details of all SSNMR experiments and simulations. This material is available free of charge via the Internet at <http://pubs.acs.org>.

■ AUTHOR INFORMATION

Corresponding Authors

loeb@uwindsor.ca

schurko@uwindsor.ca

Notes

The authors declare no competing financial interest.

■ ACKNOWLEDGMENTS

S.J.L. and R.W.S. are grateful for the awarding of NSERC of Canada Discovery grants in support of this research. S.J.L. and R.W.S. also thank the Canadian Foundation for Innovation, the

Ontario Innovation Trust, and the University of Windsor for support of the XRD and solid-state NMR facilities at the University of Windsor. Additional support was provided to S.J.L. through the NSERC Canada Research Chair (CRC) program and to R.W.S. through an Early Researcher Award (ERA) from the Province of Ontario.

■ REFERENCES

- (1) For examples of molecular switches based on MIMs see: (a) Bissell, R. A.; Cordova, E.; Kaifer, A. E.; Stoddart, J. F. *Nature* **1994**, *369*, 133. (b) Loeb, S. J.; Wisner, J. A. *Chem. Commun.* **2000**, 1939. (c) Brouwer, A. M.; Frochot, C.; Gatti, F. G.; Leigh, D. A.; Mottier, L.; Paolucci, F.; Roffia, S.; Wurpel, G. W. H. *Science* **2001**, *291*, 2124. (d) Stanier, C. A.; Alderman, J.; Claridge, T. D. W.; Anderson, H. L. *Angew. Chem.* **2002**, *114*, 1847; *Angew. Chem., Int. Ed.* **2002**, *41*, 1769. (e) Loeb, S. J.; Tiburcio, J.; Vella, S. J. *Chem. Commun.* **2006**, 1598. (f) Vella, S. J.; Tiburcio, J.; Loeb, S. J. *Chem. Commun.* **2007**, 4752. (g) Saha, S.; Flood, A. H.; Stoddart, J. F.; Impellizzeri, S.; Silvi, S.; Venturi, M.; Credi, A. *J. Am. Chem. Soc.* **2007**, *129*, 12159. (h) Stoddart, J. F. *Chem. Soc. Rev.* **2009**, *38*, 1802. (i) Balzani, V.; Credi, A.; Venturi, M. *Chem. Soc. Rev.* **2009**, *38*, 1542. (j) Ma, X.; Tian, H. *Chem. Soc. Rev.* **2010**, *39*, 70. (k) Davidson, G. J. E.; Sharma, S.; Loeb, S. J. *Angew. Chem., Int. Ed.* **2010**, *49*, 4938. (l) Altieri, A.; Aucagne, V.; Carrillo, R.; Clarkson, G. J.; D'Souza, D. M.; Dunnett, J. A.; Leigh, D. A.; Mullen, K. M. *Chem. Sci.* **2011**, *2*, 1922. (m) Evans, N. H.; Serpell, C. J.; Beer, P. D. *Chem.—Eur. J.* **2011**, *17*, 7734. (n) Carbone, A.; Goldup, S. M.; Lebrasseur, N.; Leigh, D. A.; Wilson, A. J. *Am. Chem. Soc.* **2012**, *134*, 8321. (o) Berná, J.; Alajarín, M.; Marín-Rodríguez, C.; Franco-Pujante, C. *Chem. Sci.* **2012**, *3*, 2314. (p) Grunder, S.; McGrier, P. L.; Whalley, A. C.; Boyle, M. M.; Stern, C.; Stoddart, J. F. *J. Am. Chem. Soc.* **2013**, *135*, 17691. (q) Yamada, Y.; Mihara, N.; Shibano, S.; Sugimoto, K.; Tanaka, K. *J. Am. Chem. Soc.* **2013**, *135*, 11505. (r) Dong, S.; Yuan, J.; Huang, F. *Chem. Sci.* **2014**, *5*, 247. (2) (a) Loeb, S. J. *Chem. Soc. Rev.* **2007**, *36*, 226. (b) Deng, H.; Olson, M. A.; Stoddart, J. F.; Yaghi, O. M. *Nat. Chem.* **2010**, *2*, 439. (c) Vukotic, V. N.; Loeb, S. J. *Chem. Soc. Rev.* **2012**, *41*, 5896. (d) Coskun, A.; Banaszak, M.; Astumian, R. D.; Stoddart, J. F.; Grzybowski, B. A. *Chem. Soc. Rev.* **2012**, *41*, 19. (3) Vukotic, V. N.; Harris, K. J.; Zhu, K.; Schurko, R. W.; Loeb, S. J. *Nat. Chem.* **2012**, *4*, 456. (4) (a) Vougioukalakis, G. C.; Grubbs, R. H. *Chem. Rev.* **2010**, *110*, 1746. (b) Kilbinger, A. F. M.; Cantrill, S. J.; Waltman, A. W.; Day, M. W.; Grubbs, R. H. *Angew. Chem.* **2003**, *115*, 3403; *Angew. Chem., Int. Ed.* **2003**, *42*, 3281. (c) Guidry, E. N.; Cantrill, S. J.; Stoddart, J. F.; Grubbs, R. H. *Org. Lett.* **2005**, *7*, 2129. (d) Li, S.; Liu, M.; Zheng, B.; Zhu, K.; Wang, F.; Li, N.; Zhao, X.; Huang, F. *Org. Lett.* **2009**, *11*, 3350. (e) Dasgupta, S.; Wu, J. S. *Chem. Sci.* **2012**, *3*, 425. (f) Caputo, C. B.; Zhu, K.; Vukotic, V. N.; Stephan, D. W.; Loeb, S. J. *Angew. Chem.* **2013**, *125*, 994; *Angew. Chem., Int. Ed.* **2013**, *52*, 960. (5) (a) Dybtsev, D. N.; Chun, H.; Kim, K. *Angew. Chem., Int. Ed.* **2004**, *43*, 5033. (b) Chun, H.; Dybtsev, D. N.; Kim, H.; Kim, K. *Chem.—Eur. J.* **2005**, *11*, 3521. (6) (a) Ma, B. Q.; Mulfort, K. L.; Hupp, J. T. *Inorg. Chem.* **2005**, *44*, 4912. (b) Gadzikwa, T.; Zeng, B. S.; Hupp, J. T.; Nguyen, S. T. *Chem. Commun.* **2008**, 3672. (c) Gadzikwa, T.; Farha, O. K.; Malliakas, C. D.; Kanatzidis, M. G.; Hupp, J. T.; Nguyen, S. T. *J. Am. Chem. Soc.* **2009**, *131*, 13613. (d) Farha, O. K.; Hupp, J. T. *Acc. Chem. Res.* **2010**, *43*, 1166. (e) Farha, O. K.; Malliakas, C. D.; Kanatzidis, M. G.; Hupp, J. T. *J. Am. Chem. Soc.* **2010**, *132*, 950. (f) Bury, W.; Fairen-Jimenez, D.; Lalonde, M. B.; Snurr, R. Q.; Farha, O. K.; Hupp, J. T. *Chem. Mater.* **2013**, *25*, 739. (7) (a) Chen, B. L.; Liang, C. D.; Yang, J.; Contreras, D. S.; Clancy, Y. L.; Lobkovsky, E. B.; Yaghi, O. M.; Dai, S. *Angew. Chem., Int. Ed.* **2006**, *45*, 1390. (b) Chen, B. L.; Ma, S. Q.; Zapata, F.; Fronczek, F. R.; Lobkovsky, E. B.; Zhou, H. C. *Inorg. Chem.* **2007**, *46*, 1233. (c) Park, I. H.; Kim, K.; Lee, S. S.; Vittal, J. J. *Cryst. Growth Des.* **2012**, *12*, 3397.

(8) (a) Cho, S. H.; Ma, B. Q.; Nguyen, S. T.; Hupp, J. T.; Albrecht-Schmitt, T. E. *Chem. Commun.* **2006**, 2563. (b) Mulfort, K. L.; Farha, O. K.; Stern, C. L.; Sarjeant, A. A.; Hupp, J. T. *J. Am. Chem. Soc.* **2009**, *131*, 3866. (c) Vermeulen, N. A.; Karagiaridi, O.; Sarjeant, A. A.; Stern, C. L.; Hupp, J. T.; Farha, O. K.; Stoddart, J. F. *J. Am. Chem. Soc.* **2013**, *135*, 14916.

(9) Spek, A. L. *Acta Crystallogr.* **2009**, *D65*, 148.

(10) (a) Chen, B. L.; Ma, S. Q.; Hurtado, E. J.; Lobkovsky, E. B.; Zhou, H. C. *Inorg. Chem.* **2007**, *46*, 8490. (b) Uemura, K.; Yamasaki, Y.; Komagawa, Y.; Tanaka, K.; Kita, H. *Angew. Chem., Int. Ed.* **2007**, *46*, 6662. (c) Henke, S.; Schmid, R.; Grunwaldt, J.; Fischer, R. A. *Chem.—Eur. J.* **2010**, *16*, 14296. (d) Seo, J.; Bonneau, C.; Matsuda, R.; Takata, M.; Kitagawa, S. *J. Am. Chem. Soc.* **2011**, *133*, 9005. (e) Sakata, Y.; Furukawa, S.; Kondo, M.; Hirai, K.; Horike, N.; Takashima, Y.; Uehara, H.; Louvain, N.; Meilikov, M.; Tsuruoka, T.; Isoda, S.; Kosaka, W.; Sakata, O.; Kitagawa, S. *Science* **2013**, *339*, 193.

(11) For DICVOL see: (a) David, W. I. F.; Shankland, K.; Shankland, N. *Chem. Commun.* **1998**, 931. For DASH see: (b) Boultif, A.; Louer, D. J. *Appl. Crystallogr.* **1991**, *24*, 987. (c) David, W. I. F.; Shankland, K.; van de Streek, J.; Pidcock, E.; Motherwell, W. D. S.; Cole, J. C. *J. Appl. Crystallogr.* **2006**, *39*, 910.

(12) For some relevant examples of using ²H SSNMR to probe dynamics in crystalline materials see: (a) Garcia-Garibay, M. A. *Proc. Natl. Acad. Sci. U. S. A.* **2005**, *102*, 10771. (b) Khuong, T. A. V.; Nunez, J. E.; Godinez, C. E.; Garcia-Garibay, M. A. *Acc. Chem. Res.* **2006**, *39*, 413. (c) Gould, S. L.; Tranchemontagne, D.; Yaghi, O. M.; Garcia-Garibay, M. A. *J. Am. Chem. Soc.* **2008**, *130*, 3246. (d) Morris, W.; Taylor, R. E.; Dybowsky, C.; Yaghi, O. M.; Garcia-Garibay, M. A. *Mol. Struct.* **2011**, *1004*, 94. (e) O'Brien, Z. J.; Natarajan, A.; Khan, S.; Garcia-Garibay, M. A. *Cryst. Growth Des.* **2011**, *11*, 2654. (f) Vogelsberg, C. S.; Garcia-Garibay, M. A. *Chem. Soc. Rev.* **2012**, *41*, 1892. (g) Hughs, M.; Jimenez, M.; Khan, S.; Garcia-Garibay, M. A. *J. Org. Chem.* **2013**, *78*, 5293.

(13) Ratcliffe, C. I.; Ripmeester, J. A.; Buchanan, G. W.; Denike, J. K. *J. Am. Chem. Soc.* **1992**, *114*, 3294.